Numerical and Probabilistic Methods for Modeling of Abdominal Aortic Aneurysm Rupturing Risk

Dr. Nawal Siddig[1]

[1]Affiliation:

1- Princess Nourah bint Abdulrahman University -Faculty of Sciences-Department of Mathematical sciences - Riyadh- Saudi Arabia.

2-Al Ahfad University for Women- School of Management-Sudan.

nhbs1959@gmail.com

Article Info
Page Number: 340 - 354
Publication Issue:
Vol 71 No. 2 (2022)

Abstract

This study concerns to apply numerical methods and derives a comparative Abdominal Aortic Aneurysm (AAA). An accuracy comparison has been made using the index of rupturing risk versus one computed index. The study examines some factors such as age, Mean Arterial Pressure (MAP), stress-strain via the arterial wall stress (σ), wall strength(S), and wall thickness (t). The qualms of AAA wall thickness are the most prevailing endogenous factors, as well as the wall stress and wall strength. A comparison between the Probabilistic Wall Rupture Index (PWRI), diameter-based index, and the output of the numerical method was done considering prediction power. Data records were taken from patients who underwent CT-Scan and ultrasound. Ten patients without rupturing cases were included in the statistical assessments. A matched diameter of a ruptured sample (n=7) and an unruptured sample (n=7) AAA was then considered. All the uncertainties that were observed in the thickness of the AAA wall and its strength were considered based originally on Laplace modified equation and PRRI analysis. The criteria for fitting a straight line to the data points were used for data graphing regarding the random nature of the collected data points. Statistical analysis (and plotting) of data was performed using MinitabTM, SPSSTM, and MatlabTM. The collagen-to- elastin ratio was taken as a measure of the AAA wall stiffness and tensile strength. The obtained results show that modified equations give a considerable coincide and minimum error compared with the original equation, and PRRI indicated a strong sensitivity more than the numerical models.

Article History
Article Received*: 30 December 2021*
Revised*: 06 February 2022*
Accepted*: 20 March 2022*
Publication*: 25 April 2022*

Keywords: Numerical Modeling, Abdominal, Aorta, Aneurysm, Rupture Indices, Epidemiology.

I. INTRODUCTION

A significant manifestation of cardiovascular disease involving a local dilation of any major blood vessel is called aneurysm [1] [2] [3] [4] [5] [6] [7] [8]. Conventional scanning modalities can be used for the diagnosis and follow up of any aneurysm such as ultrasonography (US), computed tomography (CT), or magnetic resonance imaging (MRI) [1] [2] [4] [6]. However, most of the aneurysm detection occurs accidentally.

Inflammation of the Aorta is termed an aortic aneurysm (AA) [1] [5]. AA can occur in either the thoracic or abdominal sections, with estimations of over a quarter-million new cases just in the United States [4] [3] [9]
Any artery can become aneurysmal, yet the infrarenal segment of the abdominal aorta is the most common site for the development of Abdominal Aortic Aneurysms (AAAs) [7] [2] [9], which would be the focus on this paper.

II. BACKGROUND

A. Diagnostic criteria

Several properties can be used for AAA detection/analysis: anatomic, radiographic, vessel wall properties and software-calculated predictive indices [4] [5] [1] [2] [7] [10] [9], some of them are presented at figure 1.

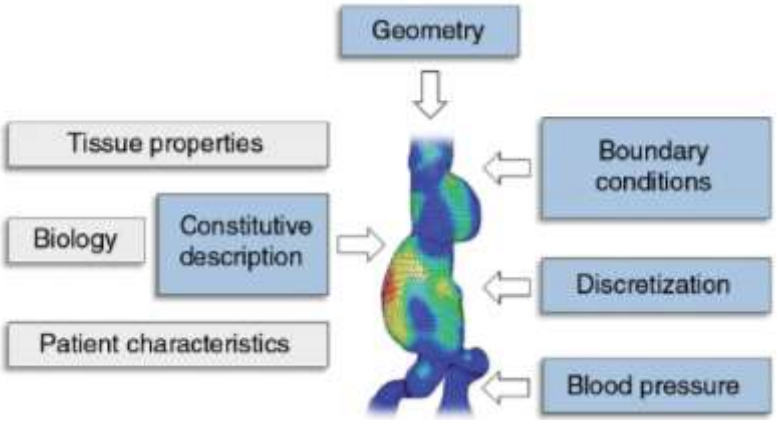

Figure 1. Clinically used criteria to assess abdominal aortic aneurysm rupture risk .

Due to the variety of criteria to determine the AAA rupture risk, the clinical community has preferences [11] [3] [5] [9] [10], shown in figure 2

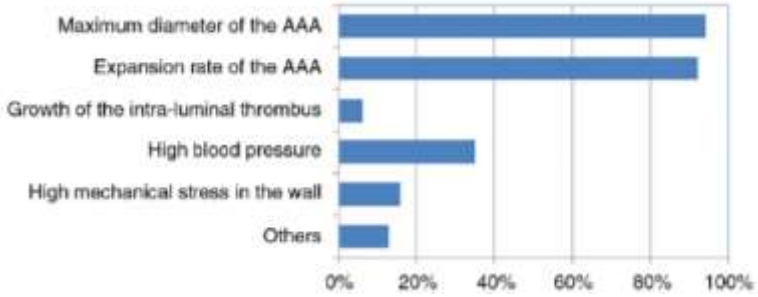

Figure 2. Criteria for determination of rupture risk of AAA .

B. Mechanical properties of AAA.

From a biomechanical point of view, AAA rupture occurs when the stress in a region of the aneurysm wall exceeds the local strength of the tissue [12] [13] [5] [14] [15]. The expansion rate of AAA per year is estimated to be 5 mm. When the maximum diameter of the aneurysm reaches 50 mm or even above, the aortic rupture can occur [1] [2] [4] [16] [17].
From a mathematical point of view, AAA integrity and rate of expansion are predicted by the matrix components of the aortic wall[1] [18] [19], [20] [14]. The aortic wall is presented in figure 3 [20].

[1] "…*The aorta belongs to the group of elastic arteries which are the ones that have relatively large diameters and are located close to the heart. Microscopically the arterial wall is composed of three distinct layers, the intima, the media and the adventitia*..." [20]

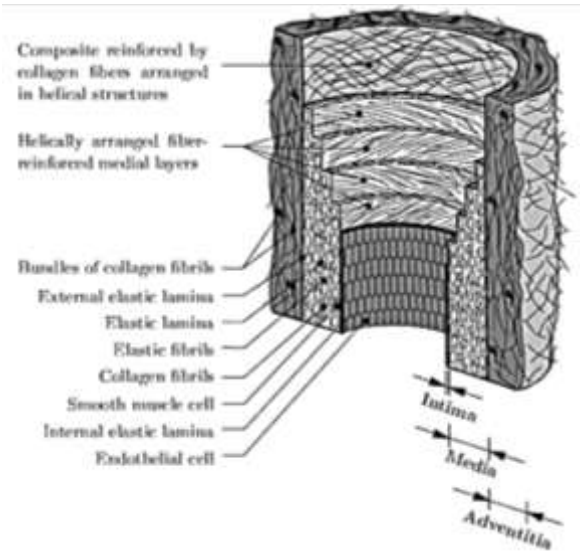

Figure 3. Diagrammatic model of the major components of a healthy elastic artery .

The AAA radius would be considered the primary independent variable that determines the rate of increase of the artery wall outwards. The most common material components that play a significant role in the aortic wall mechanics are the predominant Elastin, Collagen, and smooth- muscle cells [7] [21] [15]. "*... The latter seems to be of minor importance in the abdominal aorta ...*". [15]

Collagen-to-Elastin Ratio:

The collagen-to-elastin ratio parameter is an important measure that can be used for prediction and estimation of the dilation and stiffness of the arterial wall [15] [2] [1] [20]. The stiffness of the aorta is directly proportional to the increase of the collagen-to-elastin ratio. Also, the tensile strength of the aortic wall is inversely proportional to the mentioned ratio. It has been found that the up normal measure in the Collagen-to- Elastin ratio may not be notable during the normal pressure conditions [22] [21] [23] [15].

The relationship between the arterial stress-strain, σ, and the elevation in the collagen-to elastin ratios $\in$, is illustrated graphically in figure 4. In this case, the elastic modulus of AAA is greater than that of the normal artery, and it is clear that the curve of σ-ε moves to the left when comparing between the two cases [21] [17]

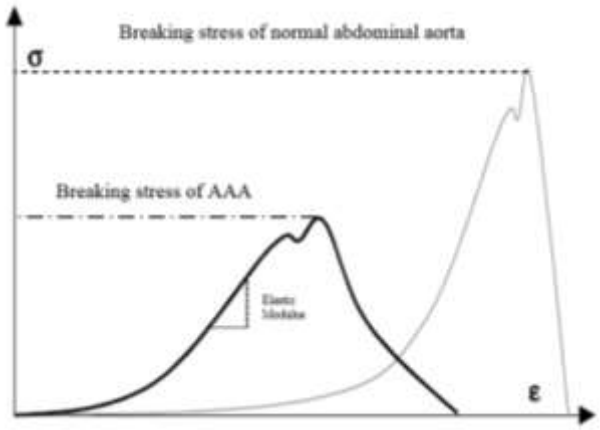

Figure 4. AAA breaking stress and a normal abdominal aorta breaking stress.

Assumptions of Aortic Wall Mechanics and Boundaries:

The Abdominal Aortic wall here is considered as a thin-walled tube that creeps under constant stress and relaxes under a constant strain in the three dimensions [4] [17] [24], as shown in figure 5.

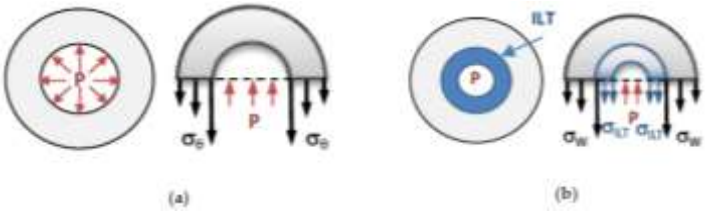

Figure 5. Stress forces acting on a perfectly cylindrical blood vessel a) Cylindrical vessel wall (gray) subjected to internal blood pressure (P) b) Cylindrical vessel wall (gray) with intraluminal thrombus /ILT, in blue) [4].

In this numerical problem, we consider the external load to be a non-axisymmetric because of AAA shape deformation. The radius is not uniform in all directions. The arterial stress-strain relationship is linear under the conditions of bounding the size of the aorta specimen into a closed curve. According to the fact that the aorta artery is a soft tissue, we can write the relationship between the uniaxial Lagrangian stress, β, and the stretch ratio, α, that affects the aorta through its three layers (intima, media, and adventitia) as [20] [1] [6]:

$$\beta = e_i\,(\alpha_2 - 1), \text{ for intima-media layer.} \quad (1)$$

$$\beta = e_0(\alpha_2 - 1)\text{ , for adventitia layer.} \quad (2)$$

Where the subscript (i) indicates the inner and (0) the outer, e_1, and e_0 are Young's moduli, in the circumferential direction [25]. This study applied biomechanical modeling and derived a computed index, which was tested against a probabilistic AAA rupture risk index for accuracy.

III. MATERIALS AND METHODS

For the numerical assessment, data were collected from King Abdullah International Medical Research Center (KAIMRC), Riyadh- Saudi Arabia, via the approval registration No.RC18/066/R in April 2018 after approval by the Department of Data Management. The study base is illustrated in table 1

No.	G.	Age	MAP (mmHg)	Pulse Rate (b/s)	CTS (cm)	Rupturing
1	M	80	163	75	8.5 × 10	No
2	M	78	176	54	6.7 × 6.12	No
3	M	81	161	72	3.2 × 5.5	No
4	M	70	209	71	5 × 2.4	No
5	M	47	160	105	5 × 4.8	No
6	M	69	196	73	5.2 × 4.6	No
7	M	59	190	87	4.3 × 4.5	No
8	F	84	190	58	4.8 × 5.8	No
9	M	55	179	83	5.8 × 8	No
10	M	55	203	58	6.5 × 10	No

Table 1. Initial CTS Records of 10 patients

The blood pressure in table 1 is taken as a MAP, which was calculated according to the following equation:

$$MAP = d_{bp} + \tfrac{1}{3}\left(s_{bp} - d_{bp}\right) \quad (3)$$

Where s_{bp} represents the systolic blood pressure, and d_{bp} is the diastolic blood pressure.

We faced some difficulties in obtaining the wall thickness of the AAA area from the available CTS records because of the lack of CTS images. Therefore, it is approximated numerically by curve fitted correlation proposed as equation 4.

$$t = 3.9 * \left[\left(\frac{Dmax}{2}\right)^{-0.2892}\right] \quad (4)$$

The output t is the wall thickness of the AAA area measured in(mm), and D_{max} the maximum diameter of AAA measured in (mm).

For minimizing the error that may occur during the temporal fluctuation of some factors, the radius here is averaged over all available measurements of CTS records, in such way:

$$r_{mean} = \frac{D_{max}+D_{min}}{4} \quad (5)$$

Since the patient's yields stress and the aneurysm wall stress are difficult to be measured, we used observational and numerical methods to compute the wall stress by using the Laplace original equation, which is defined as:

$$\sigma = \frac{MAP*r_{mean}}{C*t} \quad (6)$$

Where σ is the average wall stress, C = 1 for the cylinder.

The MAP, t, and r_{mean}, are computed from equations (3), (4), (5), respectively. The boundary conditions taken into consideration include the non-uniform nature of the geometrical shape of AAA, the influence of asymmetry, and the existence of intra-luminal thrombus (ILT). These boundary conditions make the relationship between the wall stress σ, the parameters, D_{AAA}, blood pressure, tissue properties, and others to be nonlinear.
Hence, for more accuracy, a prediction of the maximum value of the wall stress σ, defined as equation 7 is considered. Figure 6, in conjunction with equation 7, illustrates the modifications of the parameters and the geometrical shape of AAA, respectively.

$$\sigma_{max} = 0.006 \frac{(1-0.68a)e^{0.0123(0.85\mathrm{MAP}+19.5D_{max})}}{t^{0.63}b^{0.125}} \quad (7)$$

Where σ_{max} is the maximum wall stress measured in (Mpa), a is the ratio of AAA sac to ILT, D_{max} is maximum transverse diameter, b is the asymmetric index, which represents the ratio between the distance from the center point (0) to the posterior and the interior inside figure 6, and finally the systolic blood pressure (s_{bp}) [24].

The transfer's areas of AAA and ILT are calculated numerically as:

$$A_{max} = \frac{\pi D_{max} H}{4} \quad (8)$$

Where H is the in-plane axis perpendicular to D_{max}- plane, also, the lumen area is calculated in the same way, then:

$$A_{ILT} = A_{max} - A_{lumen} \quad (9)$$

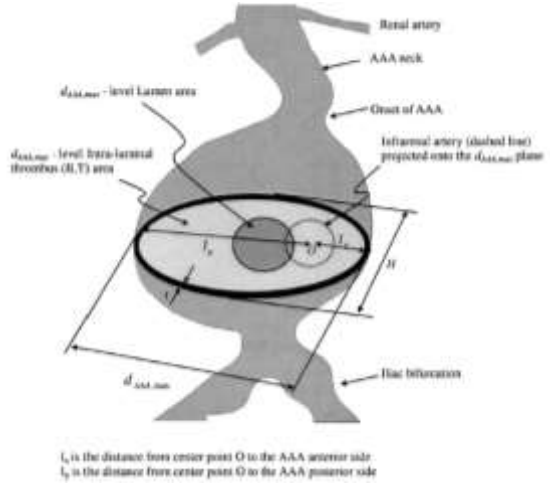

Figure 6. Geometrical Representation of AAA biomechanical parameters.

IV. RESULTS AND DISCUSSION

A. Statistical analysis:

The AAA wall was assumed to be nearly incompressible [1] [6] [26] [14], the analysis and graphics were obtained with Minitab™, Matlab™, and SPSS™

D_{max} (cm)	r_{mean} (cm)	t (mm)	σ (MPa)
10	4.6	1.2581	5.9597
6.7	3.2	1.4501	3.8839
5.5	2.2	1.4956	2.3683
5	1.85	1.5374	2.5150
5	2.45	1.5374	2.5498
5.2	2.45	1.5200	3.1591
4.5	2.2	1.5849	2.6373
5.8	2.65	1.4728	3.4187
8	3.45	1.4320	4.6018
10	4.13	1.2581	6.6683

Table 2. Biomechanical assessment outputs

The data presented for AAA at Table 2 (obtained from equations 3-6 applied on table 1) show wall thickness varying in the range [1.2,1.5] mm approximately, average wall stress higher than the clinical accepted for a normal artery [14] [13] [11] and also illustrates a linear relationship between average wall stress and radius for AAA.
A fitting analysis shows that the radius is altered gradually with age in a linear way; this coincides with some clinical outputs [3] [1] [13] [11], also relates an inverse relation between wall thickness and AAA radius. Table 1 and Table 2 show fluctuations in the relations between the MAP and the obtained mean radius. The results indicate the existence of other internal physiological factors that may interfere to some extent and affect the outcome results [6] [3] [1].

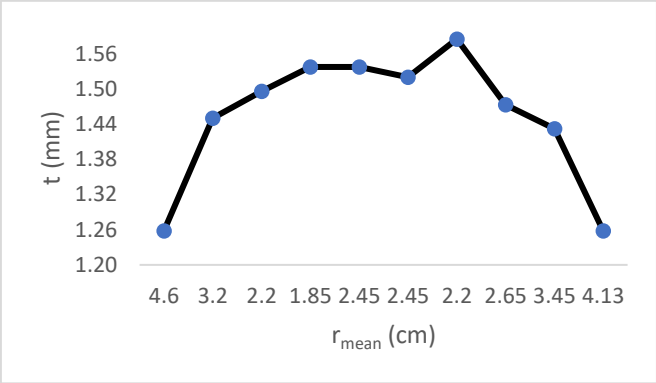

Figure 7. r_{mean} vs t

The mean radius (r_{mean}) and wall thickness (t) ,which is illustrated in figure 7,have shown an inverse linear trend also associated with Dmax. The behavior can be modeled mathematically as r_{mean}=-0.0318(t)+1.6296 with the goodness of fit (R^2) equal to 0,7279, implying a positive correlation. An alternative mathematical representation could be expressed as r_{mean}=-0,0063t^2 + 0,0378t + 1,4904 with goodness of fit (R^2) equal to 0,9121

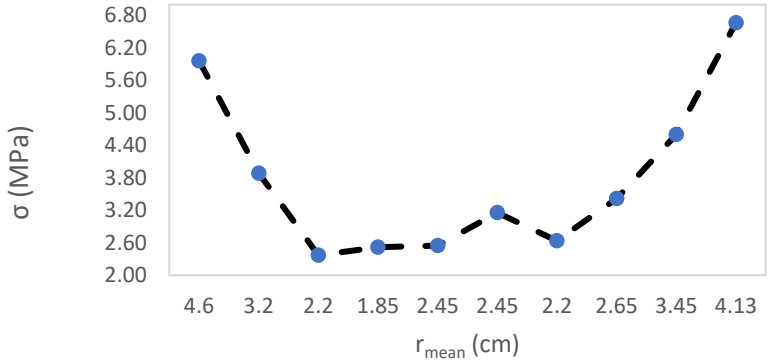

Figure 8. r_{mean} vs σ

The mean radius (r_{mean}) and average wall stress (σ) ,which is illustrated in figure 8, have shown a positive linear trend, modeled mathematically as 0,4557σ +1,27 with the goodness of fit (R^2) equal to 0,8272, implying a positive correlation. Another possible mathematical representation is $0{,}0609\sigma^2 - 0{,}2139\sigma + 2{,}6091$ with $R^2 = 0{,}9217$
Although the maximum wall stress is one of the most clinical accepted indicators for prediction of AAA risk [1] [6] [3] [27] [13] [14] [22] [18] [24], the method used for determining the values of wall stresses for different patients, sometimes is inconclusive due to the complex geometry of AAA, the impossibility to obtain in vivo stress measurements and other factors [12], [1] [6] [3] [27] [13] [14] [22] [18] [24]
During the numerical evaluation, the residual stress values were neglected, considering the small order of them. The intra-luminal material is assumed to be uniform. This may not be accurate, so it is more convenient to use the mean of ILT properties according to the exact patient-specific parameters.

B. The Estimation of the Arterial Wall Strength

For more comparative accuracy, the arterial wall Strength (S) was estimated by using a mathematical model developed by linear regression techniques, which accounts for the spatially varying influences of local ILT thickness and aneurysm wall dilation as well as other parameters. This parameter was introduced for the comparative estimation of the numerical and PRRI predictions.
By using multiple linear regression and mixed-effects modeling techniques, the final statistical model for local wall strength was given by:

$$S = 72.9 - 33.5 \times \left(\sqrt{ILT} - 079\right) - 12.3(NORD - 2.31) - 24 \times HIST + 15 \times SEX \quad (10)$$

Where S is measured in a unit of N/cm^2, ILT unit is cm, NORD is a dimensionless parameter for local normalized diameter, HIS and SEX are dimensionless binary variables (1/2 for positive family history,-1/2 for no family history), and (1/2 for males, -1/2 for females), respectively. Equation 10 had many insights regarding its physical meaning and measures in the literature.
We also defined a second measuring parameter, the Rupture Potential Index (RPI), to denote the ratio of the acting wall stress to the wall strength. Such that, the maximum value of the RPI for a particular AAA would represent the estimation of its rupture potential. When the RPI approaches a value of 1, the rupture of the AAA would be expected. The RPI may be considered to be a more reliable measuring parameter than the previously proposed measuring tools for estimating and assessing patient-specific rupture potential, even the widely accepted measures of the maximum transverse diameter. So, we define the RPI measure as the ratio of local wall stress to local wall strength; this relation is represented:

$$RPI = \frac{\sigma}{S} \quad (11)$$

Where the wall stress, σ, was estimated from the numerical prediction methods with the consideration of the measuring units. [22] [28]

C. **The Measure of the Probabilistic Rupture Risk Index (PRRI)**

Based on the same data resources, using AAA wall thickness and wall strength, the prediction was in accordance with a numerical modified Laplace equation. For more accuracy in the comparative output, we used diameter-matched samples of a ruptured group (n equal 7) and an unruptured group (n equal 7) AAAs to test the determinant power of PRRI. Individual cases were selected on purpose to obtain the best possible diameter matched groups since simple statistical confirmation is not relevant enough due to the small sizes of the selected samples in the study. For ruptured sample, blood pressure was taken from the last recording before rupture, and for un-ruptured cases at CT scanning.

The notable primary point was that the ruptured AAAs had a higher MAP. The mean difference of PRRI in the ruptured and the unruptured cases was tested. The sensitivity and the specificity of PRRI to predict rupture were analyzed to be compared with the modified numerical model.

Conferring to the AAA rupture risk hypothesis, AAA wall rupturing occurs if the wall stress surpasses the wall strength [2] [13] [12] [14]. Accordingly, the ratio of wall stress to wall strength has been used as a dimensionless local risk measure, and its peak, overall, the AAA area, was utilized as the rupture risk index. In this study, the Probabilistic wall Rupture Index (PWRI) criteria- proposed was used, which relates the local computed wall stress to the local computed wall strength. Also, AAA wall stress is computed by equation 4, and the calculated wall strength was estimated numerically by a scaled version of the model proposed by Gasser [13] and modified in detail by Gasser et al. [13] [11] [5] [7].

Regarding the fluctuation of the input information associated with every patient's historical physiology, the Peak Wall Stress (PWS) predictions were dynamically changing. For each case, the PWS followed the individual probability distribution. PRRI was integrated from the uncertainties of PWS predictions and AAA wall strength with the consideration of the definite integral:

$\int_0^{PWS} \rho_y d\rho_y$ where ρ_y is the wall strength distribution; this integral indicates that the probability of the wall strength less than a deterministic PWS value, as illustrated in figure 9.

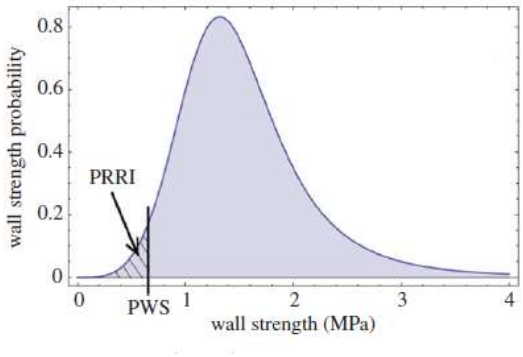

Figure 9. Deterministic PWS paired with probabilistic wall strength [14].

Then, the proposed PRRI was defined by equation 12:

$$\text{PRRI}= \int_0^{\infty} \left(\rho_{PWS} \int_0^{PWS} \rho_y d\rho_y\right) d\rho_{PWS} \quad (12)$$

Where $\int_0^{PWS} \rho_y d\rho_y$ represents the probability of wall strength.

The domain, $0 \leq PRRI \leq 1$, bound the probability of having low wall strength paired with high PWS, where a simple graphical visualization is not possible. PRRI can be computed from equation 12 by evaluating strength distribution, ρy, from in vitro testing done by [14], and the PWS distribution, ρ_{PWS} , was estimated considering the reasonable physical constraints. Then, we can select the inverse function:

$$\text{PWS (t)} = at^b \qquad (13)$$

As a response function where the power-law parameters a and b represent the least-square estimated from the discrete PWS points predicted with the modified equation of AAA (the estimated response function parameters), a and b demonstrated the selected response function of the wall stress (Intra luminal). At the same time, R showed the predicted response function. This analysis also indicated that the executed wall thicknesses should include the physical range of AAA wall thickness not to be selected too close to each other, tables 3 and 4.

Patient No.	Gender	D_{max} (mm)	Blood Pressure (mm Hg)	MAP (kPa)
1.1	Female	87	120/80	12,4
1.2	Male	70	140/90	14,2
1.3	Male	75	130/70	12
1.4	Male	75	140/80	13,3
1.5	Male	92	135/80	13
1.6	Male	67	125/75	12,2
1.7	Male	56	134/85	13,4

a) Unruptured Cases

Patient No.	Gender	D_{max} (mm)	Blood Pressure (mm Hg)	MAP (kPa)
2.1	Male	93	145/95	14,9
2.2	Male	74	120/80	12,4
2.2	Male	81	150/65	12,4
2.4	Male	67	205/85	16,5
2.5	Male	96	140/100	15,1
2.6	Male	63	160/100	16
2.7	Male	57	150/90	14,6

b) Ruptured cases

Table 3. Records of a) unruptured sample (n=7) and b) ruptured sample(n=7)

In table 3, the selected samples were validated and analyzed for PRRI. The cases of each individual were recorded to obtain the best matching diameter of the groups. The MAP here was computed as a weighted average, not arithmetic average, and was calculated as ($\frac{1}{3}$ systolic + $\frac{2}{3}$ diastolic) in the experimental pressurized steps of a finite-element model procedure done elsewhere [28] [29].

Un ruptured AAA cases

Response surface				Rupture risk parameters			
Patient No.	a (kPa)	b	R^2	PWRI	PRRI (%)	Δ(PRRI) (%)	Diam. (mm)
1.1	442	-0.487	1	0.352	0.09	0.12	67
1.2	815	-0.734	0.89	0.541	1.91	0.88	75
1.3	820	-0.894	0.91	0.386	1.65	0.77	75
1.4	822	-0.970	0.96	0.437	1.56	0.71	70
1.5	869	-1.03	0.98	2.07	1.94	0.75	87
1.6	910	-1.51	1	0.499	1.73	0.69	56
1.7	1588	-1.147	1	0.766	17.30	1.37	92

Ruptured AAA cases

Response surface				Rupture risk parameters			
Patient No.	a (kPa)	b	R^2	PWRI	PRRI (%)	Δ(PRRI) (%)	Diam. (mm)
2.1	2193	-1.17	1	2.06	37.63	1.81	93
2.2	1277	-1.108	1	0.462	9.05	1.2	74
2.3	1378	-0.382	1	1.07	28.49	3.01	81
2.4	2397	-1.438	1	1.22	36.18	1.98	67
2.5	756	-0.706	0.97	0.444	1.08	0.76	96
2.6	1748	-1.097	0.82	1.471	24.29	1.67	63
2.7	1124	-1.495	0.99	0.477	4.33	0.94	57

Table 4. Rupture Risk Index and Wall Stress information for the unruptured and the ruptured AAAs samples.

D. **Parameters a, b, R, PWRI and PRRI**

Peak wall rupture index (PWRI) was calculated from the initial ruptured sample of the patients (n=7) and the unruptured group (n=7) with the aid of equation 12. At the same time, a and b were provided together with the goodness of fit (R^2) to be in line with the deterministic in figure 9. Also, mean ΔPRRI and PRRI reflect the results obtained from the wall strength and wall thickness calculated by equations 7,8,12,13 and the aid of software (MATLAB, Minitab, and SPSS) to fit the deterministic PWS data. Figures 10, 11, and 12 show unruptured case relations for PWRI vs D_{max} , PRRi vs D_{max}, and ΔPRRI vs D_{max}, respectively.

Unruptured cases

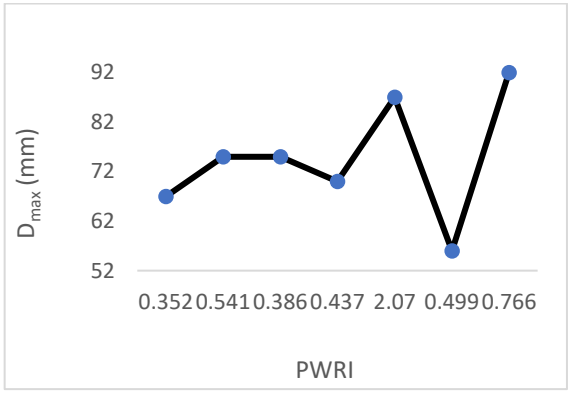

Figure 10. PWRI vs. D_{max} Data was modeled by a linear interpolation adjusted to 1,75x + 67,571 with low goodness of fit (R^2) equal to 0,0973; however, the best approximation was obtained with a fourth-grade polynomial defined by $0,5379x^4 - 7,7172x^3 + 36,167x^2 - 61,078x + 100,57$ with the goodness of fit (R^2) equal to 0,4507.

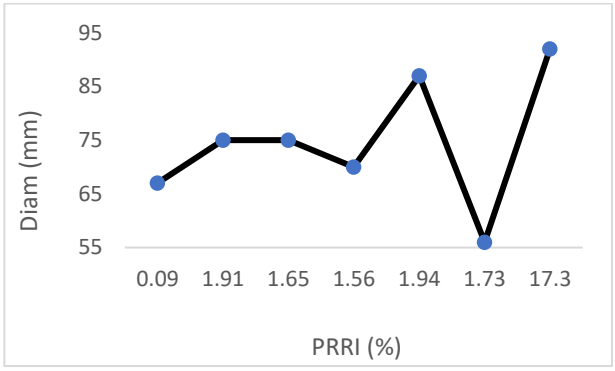

Figure 11. PRRI vs. D_{max} Data was modeled by a linear interpolation adjusted to 1,75x + 67,571 with a weak positive correlation represented by a goodness of fit coefficient (R^2) equal to 0,0973. However, a best approximation is obtained with a fourth-grade polynomial defined by 0,5379x4 - 7,7172x3 + 36,167x2 - 61,078x + 100,57 with positive correlation represented by goodness of fit (R^2) equal to 0,4507.

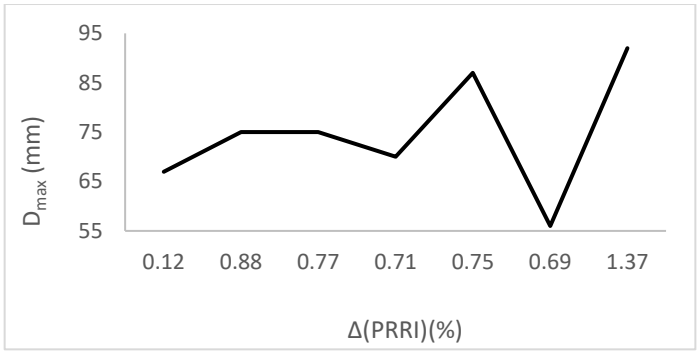

Figure 12. Δ(PRRI)(%) vs. D_{max} Data showed a linear trend modeled mathematically as 1,75 Δ(PRRI) + 67,571 with low goodness of fit equal to 0,0973. However, a best approximation is obtained with a fourth grade polynomial defined by $0,5379\ \Delta(PRRI)^4 - 7,7172\ \Delta(PRRI)^3 + 36,167\ \Delta(PRRI)^2 - 61,078\ \Delta(PRRI) + 100,57$ with goodness of fit (R^2) equal to 0,4507.

Ruptured cases

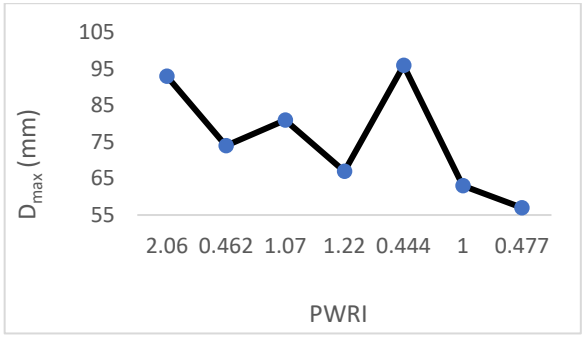

Figure 13. PWRI vs D_{max} Data behavior for ruptured AAA cases was modeled by a linear interpolation adjusted to -4,1071x + 92,286 with goodness of fit (R^2) equal to 0,3554; however, a best approximation was obtained with a fourth grade polynomial defined by $0,2652x^4 - 5,3535x^3 + 35,667x^2 - 92,572x + 155,29$ with goodness of fit (R^2) equal to 0,6016.

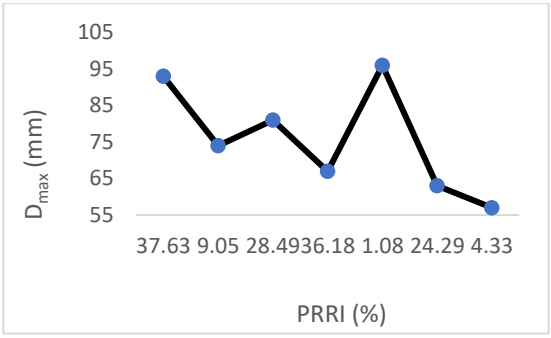

Figure 14. PRRI vs D_{max} Data behavior for ruptured AAA cases was modeled by a linear interpolation adjusted to -4,1071x + 92,286 with low goodness of fit (R^2) equal to 0,3554. However, a best approximation was obtained with a fourth-grade polynomial defined by $0,2652x^4 - 5,3535x^3 + 35,667x^2 - 92,572x + 155,29$ with goodness of fit (R^2) equal to 0,6016.

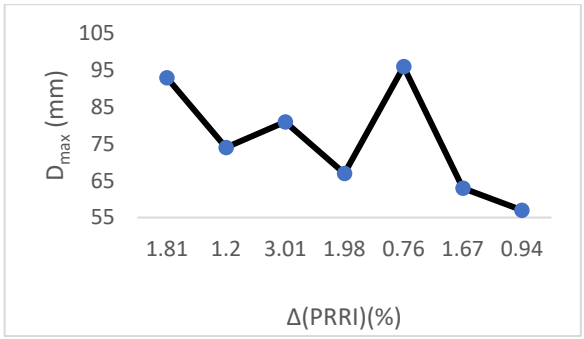

Figure 15. Δ(PRRI)(%) vs D_{max} Data behavior for ruptured AAA cases showed a linear trend modeled as -4,1071 Δ(PRRI) + 92,286 with a low goodness of fit equal to 0,3554. However a best approximation is obtained with a fourth grade polynomial defined by $0,2652\ \Delta(PRRI)^4 - 5,3535\ \Delta(PRRI)^3 + 35,667\ \Delta(PRRI)^2 - 92,572\ \Delta(PRRI) + 155,29$ with goodness of fit (R^2) equal to 0,6016

Figures 13, 14, and 15 show ruptured case relations for PWRI vs D_{max} , PRRi vs D_{max}, and ΔPRRI vs D_{max}, respectively.

		Response surface			Rupture risk parameters			
		a (kPa)	B	R^2	PWRI	PRRI (%)	Δ(PRRI) (%)	Diam. (mm)
Un ruptured cases	mean	895	-0,97	-	0,722	3,74	0,76	75
	S. D	342	0,32	-	0,61	6,01	0,37	12,12
Ruptured Cases	mean	1553	-1,28	-	1,029	20,15	1,62	76
	S. D	590	0,21	-	0,61	15,20	0,76	14,88

Table 5. Descriptive statistics from table 4

Comparative data presented in Table 5 illustrates that the mean PRRI for the ruptured sample was about five times higher than for the unruptured cases. However, the differences between the unruptured group and the ruptured group were not fully statistically significant. Graphical representations for response surface and contour plot for unruptured and ruptured cases are shown in figures 16 and 17 and figures 18 and 19, respectively.

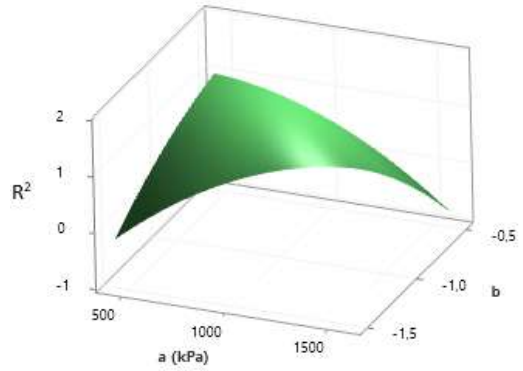

Figure 16. Response surface R^2 vs b; a (kPa) unruptured cases. The Response surface resembles a convex upward (concave function) function on 3d representation.

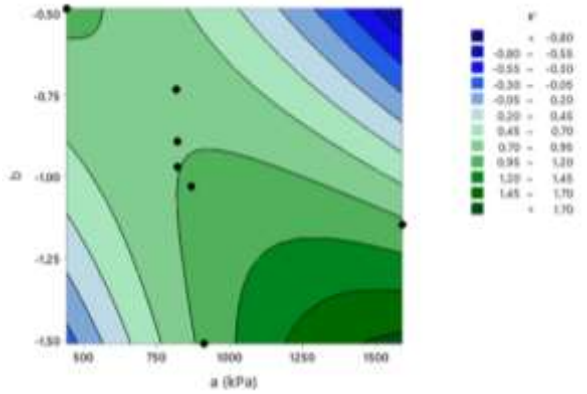

Figure 17. Contour plot. For unruptured cases, it was possible to observe that all the points belonged to the level curves in the interval [0.7, 1.20].

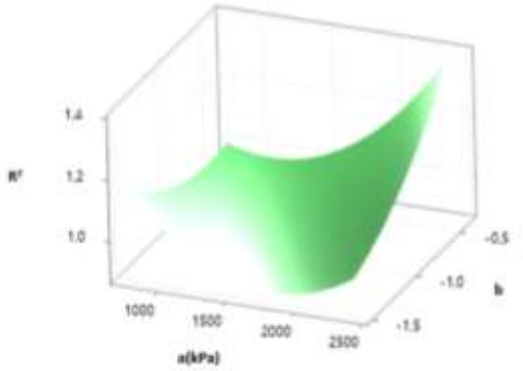

Figure 18. Response surface R^2 vs. b; a (kPa) ruptured cases. The Response surface resembles a convex downward (convex function).

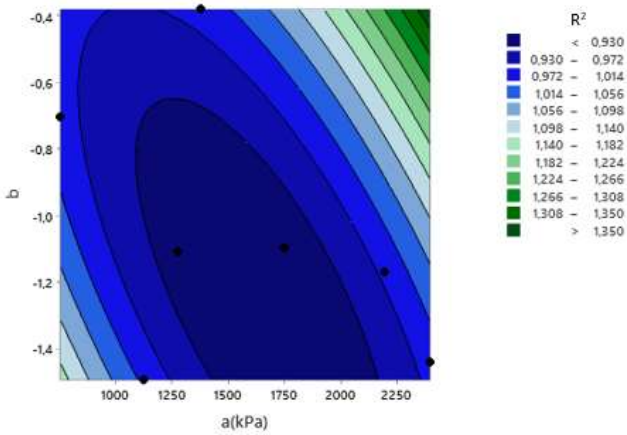

Figure 19. Contour plot. For the ruptured case, it was possible to observe that all points belonged to the level curves in the interval (<0.9, 1.014]

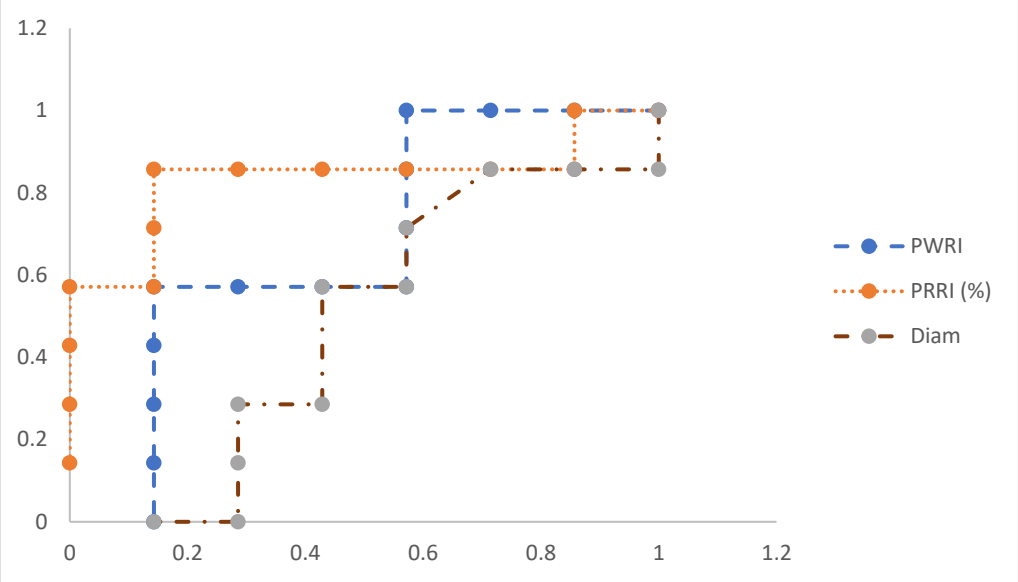

Figure 20. ROC curves for PWRI, PRRI (%), and Diam

Receiver operator characteristics (ROC) curves for PRRI (%), PWRI, and maximum diameter illustrate the false positive rate (1-specificity) and true positive rate (sensitivity) of these predictors, which are shown in figure 20. The areas under the curves, which reflect the discriminative powers of the predictors, were 0.843, 0.675, and 0.47 6, respectively, for PRRI, PWRI, and the maximum diameter.

The results of scientific research with the biomechanical approach frequently are promising; however, there are always a series of limitations due to the uncertainty of input information. The AAA biomechanics is a highly complex, and wall stress risk predictions are influenced by modeling assumptions [1] [2] [3] [4] [5] [6] [7] [11], keeping this in mind a stochastic/probabilistic criterion could have some advantages over a deterministic one.

For this work, we used a well-known probabilistic method (PWRI) [26] [14] [8], maximum diameter [1] [2] [3] [4] [5] [6] [7]. We introduced a modified PRRI index (a novel and straightforward probabilistic AAA rupture risk indicator) [11] [14] for discriminative power (accuracy) determination. The discriminative power obtained was 0.675, 0.843, and 0.476, respectively.

The newly introduced PRRI has a clear physical meaning. It also has a dependency on blood pressure. Consequently, additional information about the blood flow dynamics would directly improve the index performance.

An aorta integrity failure is a local event that is generated by a weak wall. Many weakening factors (global or local) have been reported [26] [14] [8], such as maximum diameter [1] [2] [3] [4] [5] [6] [7]. The local weakening factors can generate a highly heterogeneous wall strength, which was also indicated by heterogeneous histology of the AAA wall [4] [5]. The PRRI was computed with probabilistic, homogeneous wall strength; however, the integration of local or global weakening factors should improve the index performance. Finally, although the ROC curves reflect the computed index's accuracy superiority, it should be verified in a much larger cohort.

V. Conclusion

Uncertainties in AAA rupture behavior linked to the event's local nature and the stochastic nature of failure stimulate a generation of a probabilistic rupture index. Accounting for inhomogeneity probabilistic distributions of wall thickness and wall strength and other inputs' integrations to reduce the uncertainties could significantly improve the biomechanical AAA rupture index. Specifically, the sensitivity and the specificity of the proposed index, PRRI, were superior to the state-of-the-art biomechanical risk assessment method.

Corresponding author: Dr.NAWAL SIDDIG

Affiliation:1- Princess Nourah bint Abdulrahman University -Faculty of Sciences-Department of Mathematical sciences - Riyadh- Saudi Arabia.

2-Al Ahfad University for Women- School of Management-Sudan.

VI. REFERENCES

[1] D. Azar, D. Ohadi, A. Rachev, M. Uline e T. Shazly, "Mechanical and geometrical determinants of wall stress in abdominal aortic aneurysms: a computational study," *Plos one,* vol. 5, February 2018.

[2] A. Boyd, "Biomechanical prediction of abdominal aortic aneurysm rupture potential," *Vascular surgery,* vol. 71, nº 627, 2020.

[3] B. Doyle, N. Bappoo, M. Syed, R. Forsythe, J. Powel, N. Conlisk, P. Hoskins, G. Joldes, O. Mcbride, A. Shah, P. Norman e D. Newby, "Biomechanical assessment predicts aneurysm related events in patients with abdominal aortic aneurysm," *Journal of Vascular and Endovascular Surgery,* 2020.

[4] S. Haller, A. Azarbal e S. Rugonyi, "Predictor of abdominal aortic aneurysm risks," *Bioenginnering,* vol. 7, nº 79, 2020.

[5] T. C. Gasser, "Biomechanical rupture risk assessment A consistent and objective decision making tool for abominal aortic aneurysm patients," *Aorta,* vol. 4, nº 2, pp. 42-60, April 2016.

[6] C. A. Basciano, *Computational analysis and simulation of the non linear arterial wall dynamics with application to abdominal aortic aneurysms,* NC State University, 2007, p. 193.

[7] G. Martufi, *Biomechanics of abdominal aortic aneurysm: experimental Evidence and multiscale constitutive modelling,* KTH school of engineering sciences Department of solid mechanics, 2012.

[8] A. Siika, M. Lindquist Liljeqvist, R. Hultgren, T. C. Gasser e J. Roy, "Intraluminal thrombus is associated with early rupture of abdominal aortic aneurysm," *Journal of vascular surgery,* vol. 65, nº 4, 2016.

[9] U. Sampson, P. Norman, G. Fowkes, V. Aboyans, Y. Song, F. Harrell, M. Forouzanfar, M. Naghavi, Denenberg, Julie, F. Harrell, M. Forouzanfar, M. Naghavi, J. Denenberg, M. McDermott, M. Criui, M. Ezzati e C. Murray, "Estimation of global and regional incidence and prevalence of abdominal aortic aneurysms 1999 to 2010," *Global heart,* vol. 9, nº 1, 2014.

[10] N. Skalihasan, H. Kuivaniemi, B. Nusgens e R. D. J.-O. Durieux, "Aneurysms: epidemiolog, aetiology and pathophysiology," em *Biomechanics and mechanobiology of aneurysms*, Springer, 2011.

[11] T. C. Gasser, M. Auer, F. Labruto, J. Swedenborg e J. Roy, "Biomechanical rupture risk assessment of abdominal aortic aneurysms: model complexity versus predictability of finite element simulations," *Europeand journal of vascular and endovascular surgery,* vol. 40, pp. 176-185, 2010.

[12] Z. Li e C. Kleinstreur, "A new wall stress equation for aneurysm rupture prediction," *Annals of biomedical engineering,* vol. 33, nº 2, pp. 209-213, February 2005.

[13] T. C. Gasser, A. Nchimi, J. Swedenborg, J. Roy, N. sakalihasan, D. Bockler e A. Hyhlik-Dur, "A novel strategy to traslate the biomechanical rupture risk of abdomial aortic aneurysms to their equivalent diameter risk: method and retrospective validation," *European journal of vascular and endovascular surgery,* vol. 47, nº 3, pp. 288-295, March 2014.

[14] S. Polzer e T. C. Gasser, "Biomechanical rupture risk assessment of abdominal aortic aneurysms based on a novel probabilistic rupture risk index," *J.R.Soc interface,* vol. 12, 2015.

[15] B. Sonesson, T. Sandgren e T. Lanne, "Abdominal aortic aneurysm wall mechanics and their relation to risk of rupture," *European journal Vascular Endovascular Surgery,* vol. 18, pp. 487-493, 1999.

[16] K. Miller, H. Mufty, A. Catlin, C. Rogers, B. Saunders, R. Sciarrone, i. fourneau, b. meuris, a. tavner, g. joldes e a. wittek, "Is there a relationship between stress in wall of abdominal aortic aneurysm and symptoms ?," *Journal of surgical research,* vol. 252, pp. 37-46, August 2020.

[17] w. Hao, S. Wu, G. MR e A. e. a. Friedman, "A mathematical model of aortic aneurysm formation," *Plos one (2),* 2017.

[18] j. Urrutia, a. roy, s. raut, r. anton e s. muluk, "Geometric surrogates of abdominal aortic aneurysm wall mechanics," *Medical enginnering and physics,* pp. 1-7, 2018.

[19] I. Nordon, R. Hinchliffe, I. M. Loftus e M. M. Thompson, "Pathophysiology and epidemiology of abdominal aortic aneurysms," *Cardiology nature reviews,* vol. 8, 2011.

[20] F. R. Moyano, *Passive biomechanics of abdominal aortic aneurysms,* Universidad de Zaragoza, 2015.

[21] M. L. Raghavan, "Lecture notes on cardiovascular bio-solid mechanics section.," 2002. [Online]. [Acesso em August/28 2020 2020].

[22] M. L. Raghavan, D. A. Vorp, M. P. Federle, M. S. Makaroun e M. W. Webster, "Wall stress distributionon three dimensionally reconstructed models of human abdominal aortic aneurysm," *journal of vascular surgery,* vol. 31, nº 4, 2000.

[23] A. Shalan, j. Forsyth e A. Thompson, "Observational study comparing the measurement of abdominal aortic aneurysm (AAA) diameter in different morphology with ultrasound and CT scan," *Journal of clinical and diagnostic research,* vol. 12, nº 6, June 2018.

[24] D. Vorp, "Biomechanics of abdominal aortic aneurysm review," *Journal of biomechanics,* vol. 40, pp. 1997-1902, 2007.

[25] Y. Fung e S. Cowin, Biomechanics: mechanical properties of living tissues, American Society of Mechanical Engineers Digital Collection. Springer, 1994.

[26] P. Erhart, A. Hyhlik.Durr, P. Geisbusch, D.-E. Kotelis, T. Gasser, v. Tengg.kobligk.H e D. Bockler, "Finite element analysis in asymptomatic, symptotatic, and ruptured abdominal aortic aneurysms: in search of new rupture risk predictors," *European journal vasccular endovascular surgery,* vol. 49, pp. 239-245, 2015.

[27] D. Farotto, P. Sogers, B. meuris, J. V. Sloten e N. Famacy, "The role of biomechanics in aortic aneurysm management: requirements, open problems and future prospects," *Journal of mechanical behavior of biomedical materials,* pp. 1-45, 2017.

[28] C. Reeps, J. Pelisek, E. Hartl, V. Grabher-meier, W. Wall e M. Essler, "Measuring and modeling patient-specific distributions of material properties in abdominal aortic aneurysm wall," *Biomech model mechanobiol,* vol. 12, pp. 717-733, 2013.

[29] M. Kazi, J. Thyberg, P. Religa, J. Roy, P. Eriksson, U. Hedin e J. Swedenborg, "Influence of intraluminal thrombus on the structural and cellular composition of the abdominal aortic aneurysm wall," *Journal of vascular surgery,* vol. 38, nº 6, pp. 1283-1292, 2003.